V. Conclusion

In this paper, the uniform boundedness of the Coriolis/centripetal matrix of a serial link robot manipulator has been discussed. An easily computable explicit expression for this bound has been provided on the basis of the boundedness of the partial derivatives of the inertia matrix. The main benefit of this procedure in order to derive uniform bounds is that of avoiding the computation of the Christoffel symbols of first order and as a consequence the highly cost terms involved in the dynamics of a robot. This uniform bound can be applied to the design and tuning of several controllers proposed in the field of robotics. An example has been presented to illustrate the explicit computation of this uniform bound and a comparison with a previous result in the literature has been carried out.

References

[1] R. Gunawardana and F. Ghorbel, "On the uniform boundedness of the coriolis/centrifugal terms in the robot equations of motion," *Int. J. Robot. Automat.*, vol. 14, no. 2, pp. 45–53, 1999.

[2] B. Paden and R. Panja, "A globally asymptotically stable PD+ controller for robot manipulators," *Int. J. Control*, vol. 47, no. 6, pp. 1697–1712, 1988.

[3] S. Kawamura, F. Miyazaki, and S. Arimoto, "Is a local linear PD feedback control law effective for trajectory tracking of robot motion?," in *Proc. 1988 IEEE Int. Conf. Robot. Automat.*, Philadelphia, PA, Apr. 1988, pp. 1335–1340.

[4] R. Kelly, "Comments on: Adaptive PD controller for robot manipulators," *IEEE Trans. Robot. Automat.*, vol. 9, no. 1, pp. 117–119, Feb. 1993.

[5] P. Tomei, "Adaptive PD controller for robot manipulators," *IEEE Trans. Robot. Automat.*, vol. 7, no. 4, pp. 565–570, Aug. 1991.

[6] J. Alvarez-Ramirez, I. Cervantes, and R. Kelly, "PID regulation of robot manipulators: Stability and performance," *Syst. Contr. Lett.*, vol. 41, pp. 73–83, 2000.

[7] I. Cervantes and J. Alvarez-Ramirez, "On the PID tracking control of robot manipulators," *Syst. Contr. Lett.*, vol. 42, pp. 37–46, 2001.

[8] Z. Qu and J. F. Dorsey, "Robust PID control of robots," *Int. J. Robot. Automat.*, vol. 6, no. 4, pp. 228–235, Dec. 1991.

[9] Z. Qu and J. F. Dorsey, "Robust tracking control of robots by a linear feedback law," *IEEE Trans. Automat. Contr.*, vol. 36, no. 9, pp. 1081–1084, Sep. 1991.

[10] A. L. R. Ortega and R. Kelly, "A semiglobally stable output feedback PI2D regulator for robot manipulators," *IEEE Trans. Automat. Contr.*, vol. 40, no. 8, pp. 1432–1436, Aug. 1995.

[11] L.-L. Whitcomb, A. Rizzi, and D.-E. Koditschek, "Comparative experiments with a new adaptive controller for robot arms," *IEEE Trans. Robot. Automat.*, vol. 9, no. 1, pp. 59–70, Feb. 1993.

[12] J. T. Wen, "A unified perspective on robot control: The energy Lyapunov function approach," *Int. J. Adapt. Contr. Signal Process.*, vol. 4, pp. 487–500, 1990.

[13] B. Paden and B.-D. Riedle, "A positive-real modification of a class of nonlinear controllers for robot manipulators," in *Proc. Amer. Contr. Conf.*, Atlanta, GA, 1988, pp. 1782–1785.

[14] F. L. Lewis, C. T. Abdallah, and D. M. Dawson, *Control of Robot Manipulators*. New York: Macmillan, 1993.

[15] R. Kelly and V. Santibáñez, *Control de Movimiento de Robots Manipuladores*. Englewood Cliffs, NJ: Prentice-Hall Pearson, 2003.

[16] K. S. Fu, R. C. Gonzalez, and C. S. G. Lee, *Robotics: Control, Sensing, Vision and Intelligence*. New York: McGraw-Hill, 1986.

[17] H. Asada and J.-J. Slotine, *Robot Analysis and Control*. New York: Wiley, 1985.

[18] R. A. Horn and C. R. Johnson, *Matrix Analysis*. Cambridge, U.K.: Cambridge Univ. Press, 1999.

η^3-Splines for the Smooth Path Generation of Wheeled Mobile Robots

Aurelio Piazzi, Corrado Guarino Lo Bianco, and Massimo Romano

***Abstract*—The paper deals with the generation of smooth paths for the inversion-based motion control of wheeled mobile robots. A new path primitive, called η^3-spline, is proposed. It is a seventh order polynomial spline which permits the interpolation of an arbitrary sequence of points with associated arbitrary tangent directions, curvatures, and curvature derivatives, so that an overall G^3-path is planned. A G^3-path or path with third order geometric continuity has continuous tangent vector, curvature, and curvature derivative along the arc length. Adopting this planning scheme and a dynamic path inversion technique, the robot's command velocities are continuous with continuous accelerations. The new primitive depends on a vector (η) of six parameters that can be used to finely shape the path. The η^3-spline can generate or approximate, in a unified framework, a variety of curve primitives such as circular arcs, clothoids, spirals, etc. The paper includes theoretical results, path planning examples, and a note on general η^k-splines.**

***Index Terms*—Curve primitives, dynamic path inversion, geometric continuity, polynomial splines, smooth path generation, wheeled mobile robots.**

I. Introduction

Path planning for wheeled mobile robots (WMRs) is a long time addressed problem. At the beginnings, the research pointed at finding optimal solutions for the generation of paths joining assigned points in a planar space. Paths were made of segments and circular arcs, thus ensuring the curvature boundness, while the minimization of the curve length represented the optimality criterion to be pursued [1]–[4]. However, at the joint points between line segments and circular arcs the path curvature is discontinuous so that a WMR which follows these paths should stop in order to reorient its wheels. Hence, curvature discontinuity may be a problem in a real robotic scenario.

The advisability of pursuing a path planning with continuous curvatures for wheeled mobile robots was early indicated by Nelson [5], who proposed two path primitives, quintic curves for lane change maneuvers and polar splines for symmetric turns, to smoothly connect line segments. In the same period, also Kanayama and Hartman [6] proposed the planning with continuous curvature paths. They devised the so-called cubic spiral, a path primitive that minimizes the integral of the squared curvature variation measured along the curve. Subsequently, Delingette *et al.* [7] proposed the "intrinsic spline", a curve primitive that makes it possible to achieve overall continuous curvature and whose curvature profile is a polynomial function of the arc length.

A line of research starting with Boissonnat *et al.* [8] and continued in [9] and [10] evidenced the advisability to plan paths with a constraint on the derivative of the curvature. In a recent work [11], Fraichard and Scheuer presented a steering method, called *CC Steer*, leading to paths composed of line segments, circular arcs, and clothoids where the overall path has continuous bounded curvature and bounded curvature derivative. On the other hand, Reuter [12] went further. On the ground

Manuscript received August 3, 2006; revised January 25, 2007. This paper was recommended for publication by Associate Editor W. Burgard and Editor H. Arai upon evaluation of the reviewers' comments. This work was supported by PRIN scientific research funds of the Italian Ministry of University and Research. This paper is a revised version of a work presented at the European Control Conference, ECC'03, Cambridge, U.K., September 2003.

The authors are with the Dipartimento di Ingegneria dell'Informazione, Università di Parma, Parma 43100, Italy (e-mail: aurelio.piazzi@unipr.it).

Digital Object Identifier 10.1109/TRO.2007.903816

of avoiding jerky motions, he presented a smoothing approach to obtain trajectories with continuously differentiable curvature, i.e., both curvature and curvature derivative are continuous along the robot path.

This viewpoint was enforced by the authors in [13] where it was shown that in order to generate velocity commands with continuous accelerations for an unicycle robot, the planned path must be a G^3-path, i.e., a path with third order geometric continuity (continuity along the curve of the tangent vector, curvature, and derivative of the curvature with respect to the arc length). A path-inversion algorithm was then presented to obtain a smooth motion generation. This algorithm requires the planning of a curve satisfying geometric interpolating conditions at the endpoints that depend on the "extended state" of the WMR (Section III). This path interpolation problem was not addressed in [13] and is the subject of the present paper.

Specifically, this paper poses and solves a polynomial G^3-interpolating problem in an open unobstructed Cartesian plane. A complete solution (Section IV) is given by providing a new path primitive called $\boldsymbol{\eta}^3$-spline. This primitive, a generalization of the $\boldsymbol{\eta}^2$-spline presented in [14], is a seventh order polynomial spline that allows the interpolation of an arbitrary sequence of points with associated arbitrary tangent vectors, curvatures and curvature derivatives. In such a way, the resulting composite path is globally a G^3-path (refer to the last path planning example in Section V). The $\boldsymbol{\eta}^3$-spline depends on six parameters (grouped in vector $\boldsymbol{\eta}$) that can be freely selected to shape the curve without changing or violating the endpoint interpolation conditions. Hence, the $\boldsymbol{\eta}^3$-spline can be used to generate or approximate a variety of curve primitives such as line segments, circular arcs, clothoids, spirals, etc. (Section V).

The paper is organized as follows. Section II introduces the concept of third order geometric continuity for Cartesian curves and paths. A brief summary of the path inversion-based control of WMRs [13] is reported in Section III. Section IV proposes the polynomial G^3-interpolating problem and exposes its solution, the $\boldsymbol{\eta}^3$-spline, defined by explicit closed-form expressions (refer to (4)–(19) and Proposition 2). The new curve primitive enjoys relevant and useful properties such as completeness, minimality, and symmetry (Properties 1–3). Section V presents path generation examples. A note on the generalization of $\boldsymbol{\eta}^3$-splines is reported in Section VI. Concluding remarks in Section VII end the paper.

II. G^3-Continuity of Cartesian Curves and Paths

A curve on the $\{x, y\}$-plane can be described by the map

$$\mathbf{p} : [u_0, u_1] \to \mathbb{R}^2 \ , \ u \to \mathbf{p}\,(u) = [\alpha(u)\ \beta(u)]^T$$

where $[u_0, u_1]$ is a real closed interval. The associated "path" is the image of $[u_0, u_1]$ under the vectorial function $\mathbf{p}\,(u)$, i.e., $\mathbf{p}\,([u_0, u_1])$. We say that curve $\mathbf{p}(u)$ is regular if $\dot{\mathbf{p}}(u) \in C_p([u_0, u_1])$ and $\dot{\mathbf{p}}(u) \neq 0\ \forall u \in [u_0, u_1]$ (C_p denotes the class of piecewise continuous functions). The arc length measured along $\mathbf{p}(u)$, denoted by s, can be evaluated with the function

$$f : [u_0, u_1] \to [0, s_f] \ , \ u \to s = \int_{u_0}^{u} \|\dot{\mathbf{p}}(\xi)\|\, d\xi$$

where $\|\cdot\|$ denotes the Euclidean norm and s_f is the total curve length, so that $s_f = f(u_1)$. Given a regular curve $\mathbf{p}(u)$, the arc length function $f(\cdot)$ is continuous over $[u_0, u_1]$ and bijective; hence, its inverse is continuous too and is denoted by

$$f^{-1} : [0, s_f] \to [u_0, u_1] \ , \ s \to u = f^{-1}(s) \ .$$

Associated with every point of a regular curve $\mathbf{p}(u)$ there is the orthonormal moving frame, referred to in the following as $\{\boldsymbol{\tau}(u), \boldsymbol{\nu}(u)\}$, that is congruent with the axes of the $\{x, y\}$-plane and where $\boldsymbol{\tau}(u) = \dot{\mathbf{p}}(u)/\|\dot{\mathbf{p}}(u)\|$ denotes the unit tangent vector of $\mathbf{p}(u)$. For any regular curve such that $\ddot{\mathbf{p}}(u) \in C_p([u_0, u_1])$, the scalar curvature $\kappa_c(u)$ and the unit vector $\boldsymbol{\nu}(u)$ are well defined according to the Frenet formula $d\boldsymbol{\tau}/ds\,(u) = \kappa_c(u)\boldsymbol{\nu}(u)$ (see for example [15, p. 109]). The resulting curvature function can be then defined as

$$\kappa_c : [u_0, u_1] \to \mathbb{R} \ , \ u \to \kappa_c(u) \ .$$

The scalar curvature can be also expressed as a function of the arc length s according to the notation

$$\kappa : [0, s_f] \to \mathbb{R} \ , \ s \to \kappa(s) \ .$$

Hence, this function can be evaluated as $\kappa(s) = \kappa_c(f^{-1}(s))$.

Definition 1: (G^1-, G^2- and G^3-curves) A parametric curve $\mathbf{p}(u)$ has first order geometric continuity, and we say $\mathbf{p}(u)$ is a G^1-curve, if $\mathbf{p}(u)$ is regular and its unit tangent vector is a continuous function along the curve, i.e., $\boldsymbol{\tau}(\cdot) \in C^0([u_0, u_1])$. Curve $\mathbf{p}(u)$ has second order geometric continuity, and we say $\mathbf{p}(u)$ is a G^2-curve, if $\mathbf{p}(u)$ is a G^1-curve, $\ddot{\mathbf{p}}(\cdot) \in C_p([u_0, u_1])$, and its scalar curvature is continuous along the curve, i.e., $\kappa_c(\cdot) \in C^0([u_0, u_1])$ or, equivalently, $\kappa(\cdot) \in C^0([0, s_f])$. Curve $\mathbf{p}(u)$ has third order geometric continuity, and we say $\mathbf{p}(u)$ is a G^3-curve, if $\mathbf{p}(u)$ is a G^2-curve, $\dddot{\mathbf{p}}(\cdot) \in C_p([u_0, u_1])$, and the derivative with respect to the arc length s of the scalar curvature is continuous along the curve, i.e., $\dot{\kappa}(\cdot) \in C^0([0, s_f])$.

Barsky and Beatty [16] introduced G^1- and G^2- curves in computer graphics. G^3-curves have been recently proposed in [13] for the inversion-based control of WMRs. The related definition of G^i-paths is straightforwardly introduced as follows.

Definition 2: (G^1-, G^2-, and G^3-paths) A path of a Cartesian plane, i.e., a set of points in this plane, is a G^i-path ($i = 1, 2, 3$) or a path with ith order geometric continuity if there exists a parametric G^i-curve whose image is the given path.

Hence, G^3-paths are paths with continuously differentiable curvature. The usefulness of planning with such paths was advocated by Reuter [12] on the grounds of avoiding slippage in the motion control of wheeled mobile robots.

III. Inversion-Based Smooth Motion Control of WMRs

Consider a WMR whose nonholonomic motion model is given by

$$\begin{cases} \dot{x}(t) &= v(t)\cos\theta(t) \\ \dot{y}(t) &= v(t)\sin\theta(t) \\ \dot{\theta}(t) &= \omega(t). \end{cases} \tag{1}$$

As usual, x and y indicate the robot position with respect to a stationary frame, θ is the robot heading angle, and v and ω are its linear and angular velocities to be considered as the control inputs.

In order to achieve a smooth control, inputs $v(t)$ and $\omega(t)$ must be C^1-functions, i.e., linear and angular accelerations have to be continuous signals. It is useful to define an "extended state" of model (1) that also comprises the inputs and their first derivatives

$$\{x\,(t)\,, y\,(t)\,, \theta\,(t)\,, v\,(t)\,, \dot{v}\,(t)\,, \omega\,(t)\,, \dot{\omega}\,(t)\}\,.$$

Then, the following local smooth motion planning problem (SMPP) can be posed [13].

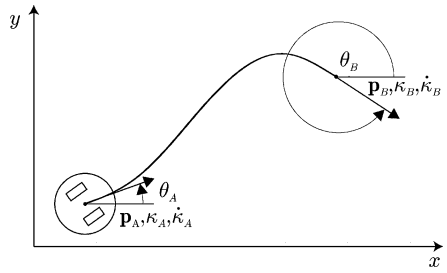

Fig. 1. G^3-path connecting $\mathbf{p}_A$ with $\mathbf{p}_B$ for the SMPP.

SMPP: Given any assigned traveling time $t_f > 0$, find control inputs $v(\cdot), \omega(\cdot) \in C^1([0, t_f])$ such that the WMR, starting from any arbitrary initial extended state

$$\mathbf{p}_A = [x_A\ y_A]^T = [x(0)\ y(0)]^T \quad \theta_A = \theta(0)$$
$$v_A = v(0) \quad \dot{v}_A = \dot{v}(0) \quad \omega_A = \omega(0) \quad \dot{\omega}_A = \dot{\omega}(0)$$

reaches any final, arbitrarily assigned, extended state

$$\mathbf{p}_B = [x_B\ y_B]^T = [x(t_f)\ y(t_f)]^T \quad \theta_B = \theta(t_f)$$
$$v_B = v(t_f) \quad \dot{v}_B = \dot{v}(t_f) \quad \omega_B = \omega(t_f) \quad \dot{\omega}_B = \dot{\omega}(t_f).$$

The solution of the above problem, exposed in [13], can be used in a motion control architecture based on the iterative steering approach [17]. In such a way, a swift high-performance motion of the WMR can be achieved, while intelligent or elaborate behaviors are performed. The solution to SMPP is based on a path dynamic inversion procedure that needs the planning of a G^3-path connecting $\mathbf{p}_A$ with $\mathbf{p}_B$. This relies on the following result.

Proposition 1: [13] Assign any $t_f > 0$. If a Cartesian path is generated by model (1) with inputs $v(t), \omega(t) \in C^1([0, t_f])$ and $v(t) \neq 0\ \forall t \in [0, t_f]$ then it is a G^3-path. Conversely, given any G^3-path there exist inputs $v(t), \omega(t) \in C^1([0, t_f])$ with $v(t) \neq 0\ \forall t \in [0, t_f]$ and initial conditions such that the path generated by model (1) coincides with the given G^3-path.

The G^3-path connecting $\mathbf{p}_A$ with $\mathbf{p}_B$ must satisfy interpolating conditions at the endpoints that depend on the initial and final extended states of the WMR. Consider, for example, the case $v_A > 0$ and $v_B > 0$. Then, angles θ_A and θ_B between the x-axis and the endpoint unit tangent vectors must coincide with the heading angles of the WMR at the initial and final poses (see Fig. 1). Moreover, curvatures and their derivatives with respect to the arc length can be determined at the endpoints according to the expressions

$$\kappa_A = \frac{\omega_A}{v_A} \quad \dot{\kappa}_A = \frac{\dot{\omega}_A v_A - \omega_A \dot{v}_A}{v_A^3}$$
$$\kappa_B = \frac{\omega_B}{v_B} \quad \dot{\kappa}_B = \frac{\dot{\omega}_B v_B - \omega_B \dot{v}_B}{v_B^3}.$$

The critical cases $v_A = 0$ and/or $v_B = 0$, as well as other cases, are discussed in [13].

Proposition 1 makes clear that continuous curvature paths, or G^2-paths, may be insufficiently smooth for a motion planning with fast and swift robot maneuvers. Indeed, with G^2-paths the command accelerations can be discontinuous causing the possible slippage of the WMR. On the contrary, G^3-paths are well suited for smooth motion planning because they can be followed with continuous accelerations commands.

IV. The η^3-Splines

In the context of smooth iterative steering for WMRs, the previous section has recalled the necessity of planning G^3-paths having arbitrary interpolating conditions at the endpoints. This justifies the introduction of the following problem.

The Polynomial G^3-Interpolating Problem: *Determine the minimal order polynomial curve which interpolates two given endpoints $\mathbf{p}_A = [x_A\ y_A]^T$ and $\mathbf{p}_B = [x_B\ y_B]^T$ with associated unit tangent vectors defined by angles θ_A and θ_B, scalar curvatures κ_A and κ_B, and curvature derivatives with respect to the arc length $\dot{\kappa}_A$ and $\dot{\kappa}_B$ (see Fig. 1). Assume that interpolating data $\mathbf{p}_A, \mathbf{p}_B \in \mathbb{R}^2$, $\theta_A, \theta_B \in [0, 2\pi)$, $\kappa_A, \kappa_B \in \mathbb{R}$ and $\dot{\kappa}_A, \dot{\kappa}_B \in \mathbb{R}$ can be arbitrarily assigned.*

The solution proposed for the above interpolating problem is given by a seventh order polynomial curve $\mathbf{p}(u) = [\alpha(u)\ \beta(u)]^T$, $u \in [0, 1]$ defined as follows:

$$\alpha(u) := \alpha_0 + \alpha_1 u + \alpha_2 u^2 + \alpha_3 u^3 + \alpha_4 u^4 + \alpha_5 u^5 + \alpha_6 u^6 + \alpha_7 u^7 \quad (2)$$
$$\beta(u) := \beta_0 + \beta_1 u + \beta_2 u^2 + \beta_3 u^3 + \beta_4 u^4 + \beta_5 u^5 + \beta_6 u^6 + \beta_7 u^7. \quad (3)$$

The polynomial coefficients are detailed by the following closed-form expressions:

$$\alpha_0 = x_A \quad (4)$$
$$\alpha_1 = \eta_1 \cos\theta_A \quad (5)$$
$$\alpha_2 = \frac{1}{2}\eta_3 \cos\theta_A - \frac{1}{2}\eta_1^2 \kappa_A \sin\theta_A \quad (6)$$
$$\alpha_3 = \frac{1}{6}\eta_5 \cos\theta_A - \frac{1}{6}\left(\eta_1^3 \dot{\kappa}_A + 3\eta_1\eta_3\kappa_A\right)\sin\theta_A \quad (7)$$
$$\begin{aligned}\alpha_4 = {} & 35(x_B - x_A) - \left(20\eta_1 + 5\eta_3 + \frac{2}{3}\eta_5\right)\cos\theta_A \\ & + \left(5\eta_1^2\kappa_A + \frac{2}{3}\eta_1^3\dot{\kappa}_A + 2\eta_1\eta_3\kappa_A\right)\sin\theta_A \\ & - \left(15\eta_2 - \frac{5}{2}\eta_4 + \frac{1}{6}\eta_6\right)\cos\theta_B \\ & - \left(\frac{5}{2}\eta_2^2\kappa_B - \frac{1}{6}\eta_2^3\dot{\kappa}_B - \frac{1}{2}\eta_2\eta_4\kappa_B\right)\sin\theta_B \end{aligned} \quad (8)$$
$$\begin{aligned}\alpha_5 = {} & -84(x_B - x_A) + (45\eta_1 + 10\eta_3 + \eta_5)\cos\theta_A \\ & - \left(10\eta_1^2\kappa_A + \eta_1^3\dot{\kappa}_A + 3\eta_1\eta_3\kappa_A\right)\sin\theta_A \\ & + \left(39\eta_2 - 7\eta_4 + \frac{1}{2}\eta_6\right)\cos\theta_B \\ & + \left(7\eta_2^2\kappa_B - \frac{1}{2}\eta_2^3\dot{\kappa}_B - \frac{3}{2}\eta_2\eta_4\kappa_B\right)\sin\theta_B \end{aligned} \quad (9)$$
$$\begin{aligned}\alpha_6 = {} & 70(x_B - x_A) - \left(36\eta_1 + \frac{15}{2}\eta_3 + \frac{2}{3}\eta_5\right)\cos\theta_A \\ & + \left(\frac{15}{2}\eta_1^2\kappa_A + \frac{2}{3}\eta_1^3\dot{\kappa}_A + 2\eta_1\eta_3\kappa_A\right)\sin\theta_A \\ & - \left(34\eta_2 - \frac{13}{2}\eta_4 + \frac{1}{2}\eta_6\right)\cos\theta_B \\ & - \left(\frac{13}{2}\eta_2^2\kappa_B - \frac{1}{2}\eta_2^3\dot{\kappa}_B - \frac{3}{2}\eta_2\eta_4\kappa_B\right)\sin\theta_B \end{aligned} \quad (10)$$
$$\begin{aligned}\alpha_7 = {} & -20(x_B - x_A) + \left(10\eta_1 + 2\eta_3 + \frac{1}{6}\eta_5\right)\cos\theta_A \\ & - \left(2\eta_1^2\kappa_A + \frac{1}{6}\eta_1^3\dot{\kappa}_A + \frac{1}{2}\eta_1\eta_3\kappa_A\right)\sin\theta_A \\ & + \left(10\eta_2 - 2\eta_4 + \frac{1}{6}\eta_6\right)\cos\theta_B \\ & + \left(2\eta_2^2\kappa_B - \frac{1}{6}\eta_2^3\dot{\kappa}_B - \frac{1}{2}\eta_2\eta_4\kappa_B\right)\sin\theta_B \end{aligned} \quad (11)$$
$$\beta_0 = y_A \quad (12)$$

$$\beta_1 = \eta_1 \sin\theta_A \tag{13}$$

$$\beta_2 = \frac{1}{2}\eta_3 \sin\theta_A + \frac{1}{2}\eta_1^2 \kappa_A \cos\theta_A \tag{14}$$

$$\beta_3 = \frac{1}{6}\eta_5 \sin\theta_A + \frac{1}{6}\left(\eta_1^3 \dot{\kappa}_A + 3\eta_1\eta_3\kappa_A\right)\cos\theta_A \tag{15}$$

$$\begin{aligned}\beta_4 = {} & 35\,(y_B - y_A) - \left(20\eta_1 + 5\eta_3 + \frac{2}{3}\eta_5\right)\sin\theta_A \\ & - \left(5\eta_1^2\kappa_A + \frac{2}{3}\eta_1^3\dot{\kappa}_A + 2\eta_1\eta_3\kappa_A\right)\cos\theta_A \\ & - \left(15\eta_2 - \frac{5}{2}\eta_4 + \frac{1}{6}\eta_6\right)\sin\theta_B \\ & + \left(\frac{5}{2}\eta_2^2\kappa_B - \frac{1}{6}\eta_2^3\dot{\kappa}_B - \frac{1}{2}\eta_2\eta_4\kappa_B\right)\cos\theta_B\end{aligned} \tag{16}$$

$$\begin{aligned}\beta_5 = {} & -84\,(y_B - y_A) + (45\eta_1 + 10\eta_3 + \eta_5)\sin\theta_A \\ & + \left(10\eta_1^2\kappa_A + \eta_1^3\dot{\kappa}_A + 3\eta_1\eta_3\kappa_A\right)\cos\theta_A \\ & + \left(39\eta_2 - 7\eta_4 + \frac{1}{2}\eta_6\right)\sin\theta_B \\ & - \left(7\eta_2^2\kappa_B - \frac{1}{2}\eta_2^3\dot{\kappa}_B - \frac{3}{2}\eta_2\eta_4\kappa_B\right)\cos\theta_B\end{aligned} \tag{17}$$

$$\begin{aligned}\beta_6 = {} & 70\,(y_B - y_A) - \left(36\eta_1 + \frac{15}{2}\eta_3 + \frac{2}{3}\eta_5\right)\sin\theta_A \\ & - \left(\frac{15}{2}\eta_1^2\kappa_A + \frac{2}{3}\eta_1^3\dot{\kappa}_A + 2\eta_1\eta_3\kappa_A\right)\cos\theta_A \\ & - \left(34\eta_2 - \frac{13}{2}\eta_4 + \frac{1}{2}\eta_6\right)\sin\theta_B \\ & + \left(\frac{13}{2}\eta_2^2\kappa_B - \frac{1}{2}\eta_2^3\dot{\kappa}_B - \frac{3}{2}\eta_2\eta_4\kappa_B\right)\cos\theta_B\end{aligned} \tag{18}$$

$$\begin{aligned}\beta_7 = {} & -20\,(y_B - y_A) + \left(10\eta_1 + 2\eta_3 + \frac{1}{6}\eta_5\right)\sin\theta_A \\ & + \left(2\eta_1^2\kappa_A + \frac{1}{6}\eta_1^3\dot{\kappa}_A + \frac{1}{2}\eta_1\eta_3\kappa_A\right)\cos\theta_A \\ & + \left(10\eta_2 - 2\eta_4 + \frac{1}{6}\eta_6\right)\sin\theta_B \\ & - \left(2\eta_2^2\kappa_B - \frac{1}{6}\eta_2^3\dot{\kappa}_B - \frac{1}{2}\eta_2\eta_4\kappa_B\right)\cos\theta_B.\end{aligned} \tag{19}$$

The real parameters η_i, $i = 1, \ldots, 6$ which appear in (4)–(19), can be freely selected and influence the path shape without violating the endpoint interpolating conditions. They can be packed together to form a six-dimensional vector $\boldsymbol{\eta} := [\eta_1\ \eta_2\ \eta_3\ \eta_4\ \eta_5\ \eta_6]^T$, and the parametric curve (2)–(3) will be concisely denoted in the following as $\mathbf{p}(u;\boldsymbol{\eta})$ or, informally, $\boldsymbol{\eta}^3$-*spline*. Vector $\boldsymbol{\eta}$ spans in $\mathcal{H} := \mathbb{R}_+^2 \times \mathbb{R}^4$.

Coefficient expressions (4)–(19) were deduced by solving a nonlinear equation system associated to the endpoint interpolation conditions. The correctness of the provided expressions is formally stated by the following proposition.

Proposition 2: The parametric curve $\mathbf{p}\,(u;\boldsymbol{\eta})$ satisfies any given set of interpolating data $\mathbf{p}_A$, θ_A, κ_A, $\dot{\kappa}_A$ and $\mathbf{p}_B$, θ_B, κ_B, $\dot{\kappa}_B$, for all $\boldsymbol{\eta} \in \mathcal{H}$.

In this paper, due to space limitations, all the formal proofs are omitted. They are reported in [18].

The next result shows how the introduced $\boldsymbol{\eta}^3$-spline is a complete parameterization of all the seventh order polynomial curves interpolating given endpoint data.

Property 1: (**Completeness**) Given any seventh order polynomial curve $\mathbf{q}(u)$, $u \in [0,1]$ with $\dot{\mathbf{q}}(0) \neq 0$ and $\dot{\mathbf{q}}(1) \neq 0$ which satisfies a given set of interpolating conditions $\mathbf{p}_A, \theta_A, \kappa_A, \dot{\kappa}_A$ and $\mathbf{p}_B, \theta_B, \kappa_B, \dot{\kappa}_B$, there exists a parameter vector $\boldsymbol{\eta} \in \mathcal{H}$ such that $\mathbf{p}(u;\boldsymbol{\eta})$ coincides with $\mathbf{q}\,(u)$.

The minimality of the $\boldsymbol{\eta}^3$-spline is the focus of the next statement.

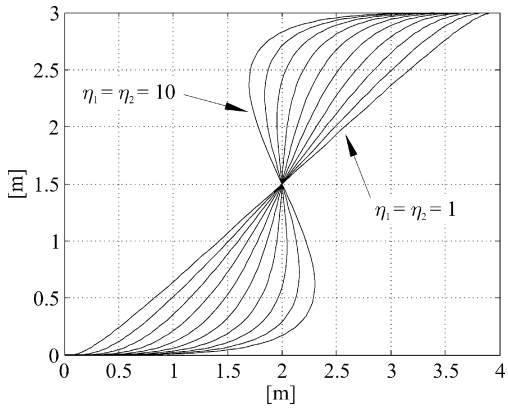

Fig. 2. Lane-change curves with $\eta_3 = \eta_4 = \eta_5 = \eta_6 = 0$.

Property 2: (**Minimality**) The curve $\mathbf{p}(u;\boldsymbol{\eta})$ is the minimal order polynomial curve interpolating any arbitrarily given set of data $\mathbf{p}_A$, $\mathbf{p}_B \in \mathbb{R}^2$, $\theta_A, \theta_B \in [0, 2\pi)$, $\kappa_A, \kappa_B \in \mathbb{R}$ and $\dot{\kappa}_A, \dot{\kappa}_B \in \mathbb{R}$.

Proposition 2 and Property 2 show that the $\boldsymbol{\eta}^3$-spline is the solution to the introduced G^3-interpolating problem. Moreover, the $\boldsymbol{\eta}^3$-spline represents a family of curves that depends on a symmetric parameterization induced by the chosen $\boldsymbol{\eta}$ vector. This property, presented formally below, may be useful in shaping the $\boldsymbol{\eta}^3$-spline by varying the η_i components.

Property 3: (**Symmetry**) Assume $\eta_1 = \eta_2 = v \in \mathbb{R}_+$, $\eta_3 = -\eta_4 = w \in \mathbb{R}$, $\eta_5 = \eta_6 = z \in \mathbb{R}$ and define $\boldsymbol{\eta} = [v\ v\ w - w\ z\ z]^T$. Moreover, consider $\theta_A = \theta_B = \theta \in [0, 2\pi)$, $\kappa_A = \kappa_B = 0$, $\dot{\kappa}_A = \dot{\kappa}_B = 0$. Then, for any $\mathbf{p}_A$ and $\mathbf{p}_B$, curve $\mathbf{p}(u;\boldsymbol{\eta})$ satisfies the following symmetry relation

$$\mathbf{p}(u;\boldsymbol{\eta}) = \mathbf{p}_A + \mathbf{p}_B - \mathbf{p}(1-u;\boldsymbol{\eta}) \tag{20}$$

$\forall u \in [0,1], \forall v \in \mathbb{R}_+, \forall w, z \in \mathbb{R}$.

The $\boldsymbol{\eta}^3$-spline can be used to generate or approximate a variety of path primitives, for example among many others, clothoids, spirals, circular arcs, etc. (see Section V). The most fundamental primitive, i.e., the line segment, can be obtained with appropriate interpolating conditions regardless of the shaping parameter $\boldsymbol{\eta}$.

Property 4: (**Line segments generation**) Define $d = \|\mathbf{p}_B - \mathbf{p}_A\|$ and assume $x_B = x_A + d\cos\theta$, $y_B = y_A + d\sin\theta$, $\theta_A = \theta_B = \theta \in [0, 2\pi)$, $\kappa_A = \kappa_B = 0$, $\dot{\kappa}_A = \dot{\kappa}_B = 0$. Then, $\mathbf{p}(u;\boldsymbol{\eta})$ is a line segment $\forall \boldsymbol{\eta} \in \mathcal{H}$.

V. Path Generation With $\boldsymbol{\eta}^3$-Splines

As shown in the previous section, the $\boldsymbol{\eta}^3$-spline depends on a vector $\boldsymbol{\eta}$ of parameters that can be freely selected to shape the spline while preserving the interpolating conditions at the path endpoints. Specifically, parameters η_1, η_3, and η_5 influence the curve at its beginning whereas η_2, η_4, and η_6 affect the curve ending. Parameters η_1 and η_2 can be interpreted as "velocity" parameters. Parameters η_3, η_4 and η_5, η_6 are "twist" parameters that depend on the curve accelerations and curve jerks at the path endpoints respectively.

Some examples illustrate the path shaping by varying the η_i parameters. Consider the following interpolating conditions that lead to symmetric lane-change curves: $\mathbf{p}_A = [0\ 0]^T$, $\mathbf{p}_B = [4\ 3]^T$, $\theta_A = \theta_B = 0$, $\kappa_A = \kappa_B = 0$, $\dot{\kappa}_A = \dot{\kappa}_B = 0$. Fig. 2 shows the influence of the velocity parameters on the curve shape by plotting ten splines with $\eta_1 = \eta_2 = 1, 2, \ldots 10$ while maintaining $\eta_3 = \eta_4 = \eta_5 = \eta_6 = 0$ for all the curves. Curves of Fig. 3 are drawn by assuming $\eta_1 = \eta_2 = 5, \eta_5 = \eta_6 = 0$ and $\eta_3 = -\eta_4 = -50, -40, \ldots, 40, 50$. They depict the effect of varying the twist acceleration parameters η_3 and η_4. Fig. 4 considers the case $\eta_1 = \eta_2 = 5, \eta_3 = -\eta_4 = 10$ and

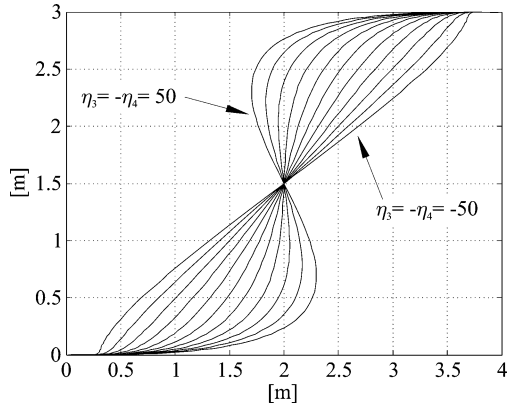

Fig. 3. Lane-change curves with $\eta_1 = \eta_2 = 5$ and $\eta_5 = \eta_6 = 0$.

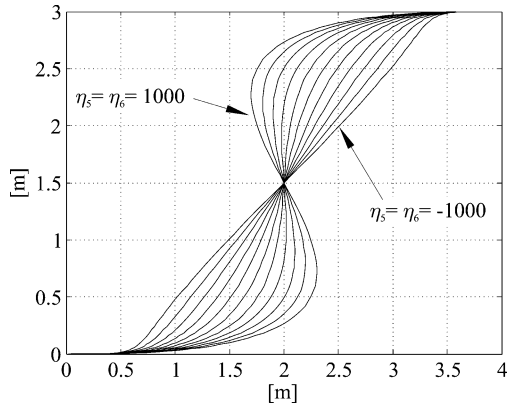

Fig. 4. Lane-change curves with $\eta_1 = \eta_2 = 5$ and $\eta_3 = -\eta_4 = 10$.

plots curves with twist jerk parameters assuming the values $\eta_5 = \eta_6 = -1000, -900, \ldots, 900, 1000$.

The proposed examples make evident that, acting on the shaping parameter vector $\boldsymbol{\eta}$, a wide variety of curves satisfying the boundary conditions can be obtained. This suggests choosing $\boldsymbol{\eta}$ to generate optimal curves. Different optimality criteria may be chosen depending on the desired WMR motion smoothness. For instance, consider a robot motion with constant linear velocity. According to the inversion-based control proposed in [13], the path arc length and the angular velocity are given by $s = vt$ and $\omega(t) = v\kappa(vt)$ with $t \in [0, t_f]$. Hence, to minimize the maximum absolute value of the angular velocity we are requested to minimize the maximum absolute value of the path curvature, i.e., to solve the problem $\min_{\boldsymbol{\eta}\in\mathcal{H}} \max_{s\in[0,s_f]} |\kappa(s;\boldsymbol{\eta})|$. Alternatively, to avoid rough movements of the WMR, we may desire to minimize the maximum absolute value of the angular acceleration along the planned path that leads to the problem

$$\min_{\boldsymbol{\eta}\in\mathcal{H}} \max_{s\in[0,s_f]} |\dot{\kappa}(s;\boldsymbol{\eta})| \ . \tag{21}$$

In many planning cases, an acceptable suboptimal solution to (21) can be obtained by a rough heuristic rule: $\eta_1 = \eta_2 = \|\mathbf{p}_A - \mathbf{p}_B\|$ and $\eta_3 = \eta_4 = \eta_5 = \eta_6 = 0$. This rule can be viewed as the straightforward extension of an analogous rule proposed in [14] for the path planning of quintic $\boldsymbol{\eta}^2$-splines (see also [19] where computational results of optimal path planning were reported). In Fig. 5, this rule has been applied to a lane-change curve with variations on the curvature derivative at the initial path point. The chosen interpolating conditions are $\mathbf{p}_A = [0\ 0]^T$, $\mathbf{p}_A = [4\ 3.5]^T$, $\theta_A = \theta_B = \pi/2$, $\kappa_a = \kappa_B = 0$, and $\dot{\kappa}_B = 0$, while the curvature derivative in $\mathbf{p}_A$ takes the values $\dot{\kappa}_A = -5, 0, 5$. According to the heuristic rule, we have chosen $\boldsymbol{\eta} = [5.3151\ 5.3151\ 0\ 0\ 0\ 0]^T$. The curves of Fig. 5 show that variations of the boundary curvature derivative may have a neat impact on the shape of the $\boldsymbol{\eta}^3$-spline.

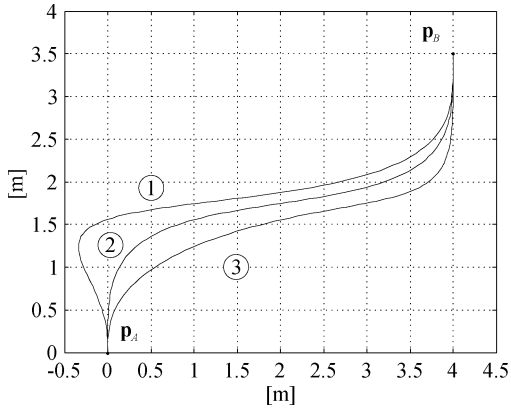

Fig. 5. Modifying a lane-change curve by perturbing $\dot{\kappa}_A$.

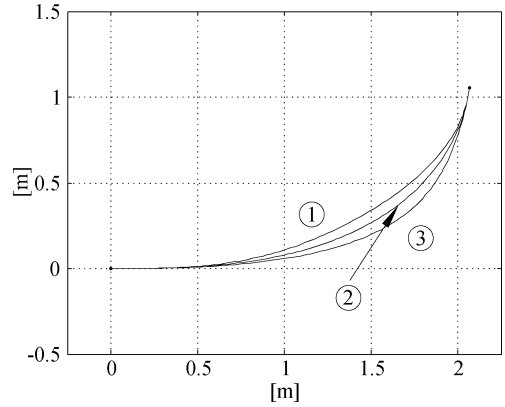

Fig. 6. Modifying a clothoid by perturbing $\dot{\kappa}_B$.

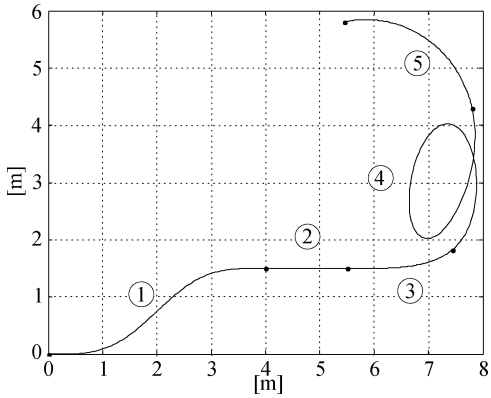

Fig. 7. Composite G^3-path made by $\boldsymbol{\eta}^3$-splines.

When appropriate endpoint interpolating conditions are chosen, the $\boldsymbol{\eta}^3$-spline can approximate a variety of primitive curves. Fig. 6 shows the plot of an $\boldsymbol{\eta}^3$-spline that is a good approximation of a clothoid (curve with label 2): it has $\dot{\kappa}(s) \simeq 0.04 \quad \forall\ s \in [0, s_f]$. The interpolating conditions are $\mathbf{p}_A = [0\ 0]^T$, $\mathbf{p}_B = [2.0666\ 1.0568]^T$, $\theta_A = 0$, $\theta_B = 1.4450$, $\kappa_A = 0$, $\kappa_B = 1.1333$, $\dot{\kappa}_A = \dot{\kappa}_B = 0.04$ and the shaping parameters have been fixed as $\eta_1 = \eta_2 = 2.37$ and $\eta_3 = \eta_4 = \eta_5 = \eta_6 = 0$. The other two curves plotted in Fig. 6 departs from the clothoid by modifying the curvature derivative in $\mathbf{p}_B$, with variation ± 0.4, so that to obtain $\dot{\kappa}_B = -0.36$ (curve 1) and $\dot{\kappa}_B = 0.44$ (curve 3).

The last example depicted in Fig. 7 reports a composite G^3-path completely generated with $\boldsymbol{\eta}^3$-splines. It is made of five curves: a lane-

TABLE I
INTERPOLATING PARAMETERS AND η_i COEFFICIENTS USED TO GENERATE THE COMPOSITE G^3-PATH

curve	$\mathbf{p}_A$	$\mathbf{p}_B$	θ_A	θ_B	κ_A	κ_B	$\dot{\kappa}_A$	$\dot{\kappa}_B$	η_1	η_2	η_3	η_4	η_5	η_6
lane-change curve	0 0	4 1.5	0	0	0	0	0	0	4.27	4.27	0	0	0	0
line segment	4 1.5	5.5 1.5	0	0	0	0	0	0	0	0	0	0	0	0
cubic spiral	5.5 1.5	7.4377 1.8235	0	0.6667	0	1	0	1	1.88	1.88	0	0	0	0
generic twirl arc	7.4377 1.8235	7.8 4.3	0.6667	1.8	1	0.5	1	0	7	10	10	-10	4	4
circular arc	7.8 4.3	5.4581 5.8064	1.8	3.3416	0.5	0.5	0	0	2.98	2.98	0	0	0	0

change curve, a line segment, a cubic spiral (i.e., a curve whose tangent direction is a cubic function of the arc length, see [6]), a generic twirl arc, and a circular arc. The interpolating and shaping parameters are reported in Table I.

VI. A NOTE ON $\boldsymbol{\eta}^k$-SPLINES

The concept of geometric continuity of planar curves and paths, introduced in Section II, can be generalized as follows (D^k denotes the kth order derivative operator).

Definition 3: (G^k-curves; $k \geq 2$) A parametric curve $\mathbf{p}(u)$ has kth order geometric continuity and we say $\mathbf{p}(u)$ is a G^k-curve if $\mathbf{p}(u)$ is G^{k-1}-curve, $D^k\mathbf{p}(\cdot) \in C_p([u_0, u_1])$, and $D^{k-2}\kappa(\cdot) \in C^0([0, s_f])$.

Definition 4: (G^k-paths; $k \geq 2$) A set of points of a Cartesian plane is a G^k-path if there exists a parametric G^k-curve whose image is the given path.

Roughly speaking, the kth order geometric continuity of curves amounts to the continuity of the curvature function up to the $(k-2)$nd derivative. In a more general setting, geometric continuity is treated in [20]. Now we can naturally state the polynomial G^k-interpolating problem as the generalization of the G^3-problem of Section IV.

The Polynomial G^k-Interpolating Problem: *Determine the minimal order polynomial curve which interpolates two given endpoints $\mathbf{p}_A = [x_A\ y_A]^T$ and $\mathbf{p}_B = [x_B\ y_B]^T$ with associated unit tangent vectors defined by angles θ_A and θ_B, and curvature derivatives $D^i\kappa_A$ and $D^i\kappa_B$ for $i = 0, 1, \ldots, k-2$. All the endpoint interpolating data can be arbitrarily assigned.*

Then, following the approach proposed in this paper, we could derive the $\boldsymbol{\eta}^k$-spline as the solution of the above problem characterized by minimality, completeness, and symmetry. For $k = 2$ this has been done in [14] and the deduced $\boldsymbol{\eta}^2$-splines are quintic polynomial curves that depend on a four-dimensional $\boldsymbol{\eta}$ vector ($\boldsymbol{\eta} \in \mathbb{R}^2_+ \times \mathbb{R}^2$ is the vector of the shaping parameters). The $\boldsymbol{\eta}^2$-splines have been proposed for autonomous guidance of cars [14] and of wheeled omnidirectional robots [21]. The remaining elementary cases ($k = 1, 0$) are reported in the Appendix.

On the grounds of the already found $\boldsymbol{\eta}^k$-splines ($k = 0, 1, 2, 3$), we infer that the general $\boldsymbol{\eta}^k$-spline is a polynomial curve with order equal to $2k+1$ and whose parameterization depends on a shaping vector $\boldsymbol{\eta}$ with $2k$ components ($\boldsymbol{\eta} \in \mathbb{R}^2_+ \times \mathbb{R}^{2(k-1)}$). Closed-form expressions of the $\boldsymbol{\eta}^k$-spline could be generated by suitably devised computer algebra procedures.

Formally define $\boldsymbol{\eta}^k$-**Paths** as the set of all the paths given by the $\boldsymbol{\eta}^k$-splines for all $\boldsymbol{\eta} \in \mathbb{R}^2_+ \times \mathbb{R}^{2(k-1)}$ and all the endpoint interpolation data. Then, the following property holds.

Property 5: $\boldsymbol{\eta}^k$-**Paths** $\subset$ $\boldsymbol{\eta}^{k+1}$-**Paths** for all $k \in \mathbb{N}$.

This property helps to explain why the $\boldsymbol{\eta}^3$-splines are quite good in approximating standard curve primitives. Indeed, it was already shown in [19] that $\boldsymbol{\eta}^2$-splines can very well approximate circular arcs or clothoids so that $\boldsymbol{\eta}^3$-splines can only better the approximations with further curve inclusions such as, for example, cubic spirals (see previous Section V). Following [13] we can foresee the use of $\boldsymbol{\eta}^4$-splines to achieve for WMRs the generation of velocity commands with continuous jerk signals (signals with continuous acceleration derivatives).

VII. CONCLUSION

The paper has presented the $\boldsymbol{\eta}^3$-spline, a seventh order polynomial curve that interpolates between two Cartesian points with arbitrary assigned tangent vectors, curvatures, and curvature derivatives. The new path primitive, given with explicit closed-form expressions, depends on a shaping parameter vector that can be freely chosen to shape or optimize the path. An advantage of the new spline over other curve primitives, such as clothoids or polynomial spirals, is the avoidance of any numerical integration/procedure to evaluate the curve coordinates. Properties of the $\boldsymbol{\eta}^3$-spline such as completeness, minimality, and symmetry have been also reported. The paper has concentrated on smooth path planning in an unobstructed space and has not addressed the obstacle-avoidance issue. To achieve obstacle-avoidance capabilities, as shown in [22], the $\boldsymbol{\eta}^3$-spline can be used as a flexible local path planner within a probabilistic global path planner.

APPENDIX

Case $k = 1$ (solution to the polynomial G^1-interpolating problem). The $\boldsymbol{\eta}^1$-spline is a third order polynomial curve $\mathbf{p}(u;\boldsymbol{\eta})\ u \in [0,1]$, $\boldsymbol{\eta} = [\eta_1 \eta_2]^T \in \mathbb{R}^2_+$ with coefficients defined as follows:

$$\begin{aligned}
\alpha_0 &= x_A \\
\alpha_1 &= \eta_1 \cos\theta_A \\
\alpha_2 &= 3\,(x_B - x_A) - 2\eta_1 \cos\theta_A - \eta_2 \cos\theta_B \\
\alpha_3 &= -2\,(x_B - x_A) + \eta_1 \cos\theta_A + \eta_2 \cos\theta_B \\
\beta_0 &= y_A \\
\beta_1 &= \eta_1 \sin\theta_A \\
\beta_2 &= 3\,(y_B - y_A) - 2\eta_1 \sin\theta_A - \eta_2 \sin\theta_B \\
\beta_3 &= -2\,(y_B - y_A) + \eta_1 \sin\theta_A + \eta_2 \sin\theta_B.
\end{aligned}$$

Case $k = 0$ (solution to the polynomial G^0-interpolating problem). For completeness we also give the $\boldsymbol{\eta}^0$-spline which is simply expressed by the first-order curve $\mathbf{p}(u) = \mathbf{p}_A + \mathbf{p}_B \cdot u,\ u \in [0,1]$. There are no shaping parameters as the curve is just the line segment connecting $\mathbf{p}_A$ with $\mathbf{p}_B$. Note that zero-order geometric continuity coincides with the standard notion of function continuity (C^0-continuity).

REFERENCES

[1] L. Dubins, "On curves of minimal length with a constraint on average curvature and with prescribed initial and terminal positions and tangents," *Amer. J. Math.*, vol. 79, pp. 497–517, 1957.

[2] J. Reeds and R. Shepp, "Optimal paths for a car that goes both forward and backward," *Pacific J. Math.*, vol. 145, no. 2, pp. 367–393, 1990.

[3] J.-D. Boissonnat, A. Cérézo, and J. Leblond, "Shortest paths of bounded curvature in the plane," in *Proc. 1992 IEEE Int. Conf. Robot. Automat.*, Nice, France, May 1992, pp. 2315–2320.
[4] P. Souères and J.-P. Laumond, "Shortest paths synthesis for a car-like robot," *IEEE Trans. Automat. Contr.*, vol. 41, no. 5, pp. 672–688, May 1996.
[5] W. Nelson, "Continuous steering-function control of robot carts," *IEEE Trans. Ind. Electron.*, vol. 36, no. 3, pp. 330–337, Aug. 1989.
[6] Y. Kanayama and B. Hartman, "Smooth local path planning for autonomous vehicles," in *Proc. IEEE Int. Conf. Robot. Automat.*, Scottsdale, AZ, May 1989, vol. 3, pp. 1265–1270.
[7] H. Delingette, M. Hébert, and K. Ikeuchi, "Trajectory generation with curvature constraint based on energy minimization," in *Proc. IEEE/RSJ Int. Conf. Intell. Robots Syst.*, Osaka, Japan, Nov. 1991, pp. 206–211.
[8] J.-D. Boissonnat, A. Cérézo, and J. Leblond, "A note on shortest paths in the plane subject to a constraint on the derivative of the curvature," INRIA, Rocquencourt, France, Tech. Rep. 2160, 1994.
[9] A. Scheuer and C. Laugier, "Planning sub-optimal and continuous-curvature paths for car-like robots," in *Proc. 1998 IEEE/RSJ Int. Conf. Intell. Robots Syst.*, Victoria, BC, Canada, Oct. 1998, pp. 25–31.
[10] T. Kito, J. Ota, R. Katsuki, T. Mizuta, T. Arai, T. Ueyama, and T. Nishiyama, "Smooth path planning by using visibility graph-like method," in *Proc. IEEE Int. Conf. Robot. Automat.*, Taipei, Taiwan, R.O.C., 2003, pp. 3770–3775.
[11] T. Fraichard and A. Scheuer, "From Reeds and Shepp's to continuous-curvature paths," *IEEE Trans. Robotics*, vol. 20, no. 6, pp. 1025–1035, Dec. 2004.
[12] J. Reuter, "Mobile robots trajectories with continuously differentiable curvature: An optimal control approach," in *Proc. 1998 IEEE/RSJ Int. Conf. Intell. Robots Syst.*, Victoria, BC, Canada, Oct. 1998, vol. 1, pp. 38–43.
[13] C. Guarino, L. Bianco, A. Piazzi, and M. Romano, "Smooth motion generation for unicycle mobile robots via dynamic path inversion," *IEEE Trans. Robotics*, vol. 20, no. 5, pp. 884–891, Oct. 2004.
[14] A. Piazzi, C. Guarino Lo Bianco, M. Bertozzi, A. Fascioli, and A. Broggi, "Quintic G^2-splines for the iterative steering of vision-based autonomous vehicles," *IEEE Trans. Intell. Transport. Syst.*, vol. 3, no. 1, pp. 27–36, Mar. 2002.
[15] C.-C. Hsiung, *A First Course in Differential Geometry*. Cambrige, MA: International Press, 1997.
[16] B. A. Barsky and J. C. Beatty, "Local control of bias and tension in beta-spline," *Comput. Graph.*, vol. 17, no. 3, pp. 193–218, 1983.
[17] P. Lucibello and G. Oriolo, "Stabilization via iterative state steering with application to chained-form systems," in *Proc. 35th IEEE Conf. Decision Contr.*, Kobe, Japan, Dec. 1996, vol. 3, pp. 2614–2619.
[18] A. Piazzi, C. Guarino Lo Bianco, and M. Romano, "Smooth path generation for wheeled mobile robots using η^3-splines," Università di Parma, Dipt. Ingegneria dell'Informazione, Parma, Italy, Tech. Rep. TSC01/07, 2007.
[19] C. Guarino Lo Bianco and A. Piazzi, "Optimal trajectory planning with quintic G^2-splines," in *Proc. IEEE Intell. Veh. Symp. (IV2000)*, Dearborn, MI, Oct. 2000, pp. 620–625.
[20] J. Peters, "Geometric continuity," in *Handbook of Computer Aided Geometric Design*, G. Farin, J. Hoschek, and M.-S. Kim, Eds. Amsterdam, The Netherlands: North-Holland, 2002, pp. 193–229.
[21] C. Guarino Lo Bianco, A. Piazzi, and M. Romano, "Smooth control of a wheeled omnidirectional robot," presented at the IFAC Symp. Intell. Autonom.Veh., IAV2004, Lisbon, Portugal, Jul. 2004.
[22] J. Villagra and H. Mounier, "Obstacle-avoiding path planning for high velocity wheeled mobile robots," presented at the IFAC World Congr., Prague, Czech Republic, Jul. 2005.

Cooperative Motion Control and Sensing Architecture in Compliant Framed Modular Mobile Robots

Xiaorui Zhu, Youngshik Kim, Roy Merrell, and Mark A. Minor

***Abstract*—A novel motion control and sensing architecture for a two-axle Compliant Framed wheeled Modular Mobile Robot (CFMMR) is proposed in this paper. The CFMMR is essentially a cooperative mobile robotic system with complex physical constraints and highly nonlinear interaction forces. The architecture combines a kinematic controller for coordinating motion and providing reference commands, robust dynamic controllers for following these commands and rejecting disturbances, and a sensor fusion system designed to provide accurate relative posture estimates. Requirements for each of these subsystems and their respective interconnections are defined in this paper in order to optimize system performance. Experimental results compare performance of the proposed architecture to sub-optimal configurations. Results derived from seven groups of experiments based upon 35 individual tests validate superiority of the architecture.**

***Index Terms*—Cooperative systems, distributed control, motion control, robot sensing systems, tracking.**

I. Introduction

Cooperative motion control and sensing for Compliant Framed wheeled Modular Mobile Robots (CFMMR) (Fig. 1) is the focus of this research. The CFMMR uses compliant frame members to couple rigid axle modules with independently controlled wheels [1]. Wheel commands are used to deform the frame for advanced steering capability. Frame compliance also allows the robot to twist its shape and adapt to rugged terrain. Simplicity and modularity of the system emphasize its cost effectiveness, durability in adverse climates, and capability to be reconfigured for a multitude of applications.

A number of cooperative wheeled mobile robots have been investigated in recent decades. A detailed comparison is described in [1], [2]. Most similar of these is the snake-like robot Genbu [3], which uses entirely passive joints to allow cooperation amongst wheel axles for adaptation to uneven terrain. However, motion control of [3] focused on the simple posture alignment and functional ability [3], [4] while this paper deals with general navigation issues and accurate motion control.

In this paper, we propose a new sensing and control architecture in order for the system to be scalable, distributed, and cooperative. The architecture (Fig. 2) consists of kinematic (K) control, dynamic (D) control, and sensing (S) systems components. In this architecture, each axle module is treated individually as an autonomous mobile

Manuscript received September 5, 2006; revised January 9, 2007. This paper was recommended for publication by Associate Editor S. Ma and Editor H. Arai upon evaluation of the reviewers' comments. This work was supported by the National Science Foundation under NSF Grant IIS-0308056. This paper was presented in part at the International Conference on Robotics and Automation, Orlando, FL, 2006, and in part at the International Conference on Advanced Intelligent Mechatronics, Monterey, CA, 2005.

X. Zhu was with the Department of Mechanical Engineering, University of Utah, Salt Lake City, UT 84112 USA. She is now with Harbin Institute of Technology at Shenzhen, Shenzhen, Guangdong 518055, China (e-mail: xiaoruizhu@hitsz.edu.cn)

Y. Kim and M. A. Minor are with the Department of Mechanical Engineering, University of Utah, Salt Lake City, UT 84112 USA (e-mail: youngshik.kim@utah.edu; minor@mech.utah.edu).

R. Merrell was with the Department of Mechanical Engineering, University of Utah, Salt Lake City, UT 84112 USA. He is now with ATK Launch Systems, Magna, UT 84044 USA (e-mail: mailroy@excite.com).

Color versions of one or more of the figures in this paper are available online at http://ieeexplore.ieee.org.

Digital Object Identifier 10.1109/TRO.2007.903815